Spectrally undiscerned isomers might lead to erroneous determination of water exchange rates of paraCEST Eu(III) agents

Nevenka Cakic[a], Ben Tickner[a], Moritz Zaiss[b], David Esteban-Gómez[c], Carlos Platas-Iglesias[c*] and Goran Angelovski[a†]

[a] MR Neuroimaging Agents, Max Planck Institute for Biological Cybernetics, 72076 Tübingen, Germany

[b] High-Field Magnetic Resonance, Max Planck Institute for Biological Cybernetics, 72076 Tübingen, Germany

[c] Universidade da Coruña, Centro de Investigacións Científicas Avanzadas (CICA) and Departamento de Química Fundamental, Facultade de Ciencias, 15071 A Coruña, Galicia, Spain

Inorganic Chemistry, volume 56, issue 14, pages 7737–7745, 17 July 2017
Received 18 February 2017, published online 23 June 2017, published in print 17 July 2017

How to cite:

Spectrally Undiscerned Isomers Might Lead to Erroneous Determination of Water Exchange Rates of paraCEST Eu(III) Agents. Nevenka Cakić, Ben Tickner, Moritz Zaiss, David Esteban-Gómez, Carlos Platas-Iglesias, and Goran Angelovski. *Inorganic Chemistry* **2017** *56* (14), 7737-7745. DOI: 10.1021/acs.inorgchem.7b00441.

Abstract

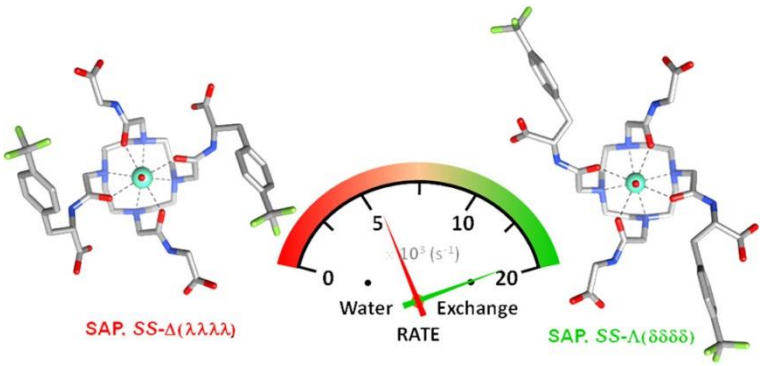

We report a detailed study of the solution structure and water exchange rate of a Eu(III) complex with the cyclen-based ligand **L**[1], containing (*S*)-2-(2-acetamido)-3-(4-(trifluoromethyl)phenyl)propanoate pendant arms at positions 1 and 7 of the cyclen ring and acetylglycinate pendants at positions 4 and 10. The **EuL**[1] complex was characterized by a combination of NMR and luminescence spectroscopy and density functional theory (DFT) calculations. The chemical exchange saturation transfer (CEST) spectra obtained at different temperatures and saturation powers present a CEST signal attributed to the coordinated water molecule. However, the spectra recorded at low temperatures (10 °C) and low saturation powers revealed the presence of two different species with coordinated water molecules having very similar chemical shifts. Determination of the water exchange rates of the coordinated water molecules was carried out by using the Bloch four-pool model that accounts for the presence of these isomers, and this model was compared to conventional methods for CEST quantification, namely the Omega plot and QUESP (quantification of

* carlos.platas.iglesias@udc.es
† goran.angelovski@tuebingen.mpg.de

exchange rate as a function of saturation power), which assume the presence of a single CEST active species. The results indicated that only the four-pool Bloch equations provide reasonable water exchange rates and activation parameters. Solution NMR studies and DFT calculations indicated that the two isomers present in solution correspond to the *SS*-Δ(λλλλ) and *SS*-Λ(δδδδ) isomers, which present capped square-antiprismatic (SAP) coordination environments. Additional NMR studies on the **EuL^2** and **EuL^3**complexes, which present four (*S*)-2-(2-acetamido)-3-(4-(trifluoromethyl)phenyl)propanoate or acetylglycinate pendant arms, respectively, confirm the results obtained for **EuL^1**.

Keywords: paraCEST; DFT calculations; lanthanide complexes; cyclen; water exchange rates

Introduction

The extensive use of magnetic resonance imaging (MRI), one of the most widely accepted biomedical tools nowadays, has resulted in the development of various types of contrast agents (CAs). They increase the sensitivity and specificity of MRI scans and aid obtaining important insights into the biological states of tissues and organs. While a great deal of work has already been done on the development of CAs, a need for their improvement and optimization still persists. For instance, conventional paramagnetic gadolinium-based complexes operate at the frequency of protons and are suitable for T_1-weighted MRI. Here, the preparation of high-relaxivity T_1 agents appears to be the greatest challenge.[1] On the other hand, heteronuclear contrast agents such as those suitable for ^{19}F MRI are also regarded as promising substitutes for Gd-based CAs. The absence of a background signal, high sensitivity relative to protons, and easy retuning of instruments from proton to fluorine frequency are the main reasons for utilization of ^{19}F-based agents.[2] However, since the signal intensity depends on agent concentration, attempts to increase the number of ^{19}F atoms in the molecule cause issues with aqueous solubility and shortening of T_2 triggered by the increase in molecular size.[3] To further circumvent the issues related to the performance of CAs, various alternatives are being developed using the same nuclei but different mechanisms to obtain the MR signal.

The chemical exchange saturation transfer (CEST) technique belongs to such alternatives and is appreciated due to the possibility of turning the contrast on and off at will by simple activation of the CEST contrast agents with a radio frequency (RF) pulse.[4] Namely, in order to create CEST contrast, a frequency-selective presaturation RF pulse is applied to a pool of protons that is in slow to intermediate exchange with bulk water protons, thereby decreasing the magnetization of these exchanging protons. The exchange of protons between these two types of molecules alters the image contrast by reducing the magnetization and hence the MRI signal intensity of the tissue water. However, in order to observe a CEST effect, the frequency difference between the two pools of protons ($\Delta\omega$) must be higher than or equal to the exchange rate between the pools (k_{ex}). Furthermore, k_{ex} should be in a slow regime to allow utilization of low RF power, necessary for *in vivo* CEST MRI experiments.[5]

Paramagnetic complexes, in particular lanthanide-based species, offer a good platform for the preparation of paramagnetic CEST (paraCEST) contrast agents that are well suited to CEST MRI purposes.[6] Indeed, the majority of lanthanide ions are also known as NMR shifting agents,[7,8] thus increasing the $\Delta\omega$ value between exchangeable protons and bulk water, making it easier to attain the $\Delta\omega \geq k_{ex}$ condition (see above). Concurrently, this shift in proton frequency also eliminates interferences of the CEST effect generated by the paraCEST CA from other existing diamagnetic CEST processes within the tissue. Finally, a large choice of paramagnetic ions offers a wide range of possibilities for adjustment of the frequency shift of exchangeable protons, as well as tuning of their exchange rates.

To this end, a large number of different types of paraCEST CAs have been prepared and analyzed in the past decade.[6,9] However, those suited for optimal CEST detection, i.e. with slow exchange rates, are quite seldom. Recently, Sherry and co-workers introduced complexes that exhibit lower exchange rates in comparison to

any previous paraCEST CA.[10] These complexes are appended with glutamyl-phosphonate side arms, and their k_{ex} values are in the range of ~1500–2000 Hz (water residence lifetime ~500–700 μs) due to the presence of ethyl ester protected phosphonate groups which reduce the exchange of the inner-sphere water molecule coordinated to Eu(III) with the bulk water molecules. On the other hand, we postulated that appending hydrophobic fluorine-containing aryl groups on the Eu(III) complex may result in paraCEST agents with slow exchange rates. Furthermore, the presence of fluorine atoms would result in an agent suitable for multicontrast MRI, namely for ^{1}H T_1, ^{1}H CEST, and ^{19}F MRI.[11] Nevertheless, in view of the recently communicated revisited methodology for accurate quantification of CEST (qCEST),[12] our initially reported k_{ex} values for the aforementioned multicontrast MRI agent appeared to be different from those calculated by the qCEST method for the same system. We therefore sought to investigate the new system more thoroughly, perform revised qCEST calculations, and determine the major reasons for mismatched values. In this work, we report the insights obtained from investigating the coordination chemistry of two complexes **EuL^{1,2}** appended with 4-(trifluoromethyl)-l-phenylalanine (*p*-CF_3-Phe) groups and the reflection of these coordination properties on the CEST effect. The difference between complexes **EuL^{1,2}** is the number of hydrophobic groups incorporated into the final chelate, namely two *p*-CF_3-Phe groups in trans positions and four groups for **EuL^{1}** and **EuL^{2}**, respectively (Chart 1). The preliminary ^{19}F NMR data reported for **EuL^{1}** indicated the presence of different isomers in solution,[11] which is likely related to the presence of stereogenic centers at the amide side chains. Indeed, previous studies demonstrated that the presence of chiral centers resulted in diastereoisomers having very different water exchange rates.[13-15] Thus, herein we evaluate the effect that the presence of different isomers has on the water exchange rates obtained using different methods. In particular, our motivation for this work was to develop the methodology to examine accurately the water exchange rates of the different species in aqueous media. For this purpose we used variable-temperature studies to extract water exchange rates and the associated activation parameters. The obtained results were compared to a golden standard Eu(III) complex derived from DOTA-tetraglycineamide (DOTAM-Gly, **EuL^{3}**).

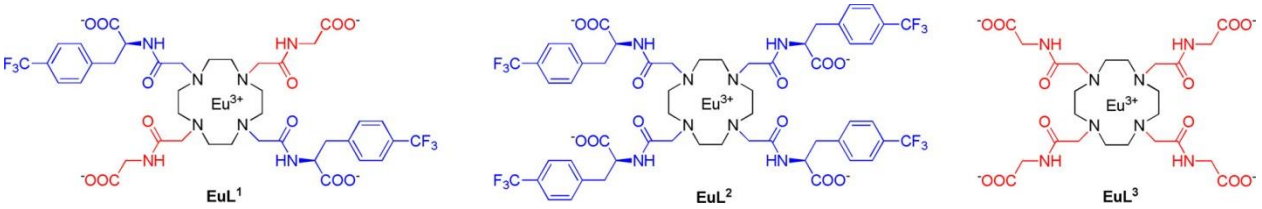

Chart 1. Structures of Complexes **EuL$^{1–3}$** Investigated in This Study.

Results and Discussion

Preparation of the Complexes

EuL^{1} and **EuL^{3}** were prepared according to previously published procedures.[11,16] The complex with four *p*-CF_3-Phe groups, **EuL^{2}**, was prepared analogously to **EuL^{1}** by using cyclen (**1**) and (*S*)-2-(2-chloroacetylamino)-3-(4-trifluoromethylphenyl)propionic acid ethyl ester (**2**; Scheme 1). Namely, cyclen was alkylated with chloride **2** in acetonitrile using potassium carbonate as base. The ethyl esters in the resulting tetraalkylated macrocycle were hydrolyzed with sodium hydroxide in a solvent mixture composed of tetrahydrofuran/ethanol/water to yield the ligand **L^{2}**.

Unlike **L^{1}**, the chelator **L^{2}** exhibited poor solubility in water, likely due to the presence of many hydrophobic groups within the molecule. Therefore, the preparation of its lanthanide complexes (Eu(III), Yb(III), Dy(III)) had to be performed in a mixture of EtOH and H_2O. Obviously, the presence of four hydrophobic *p*-CF_3-Phe

groups strongly influences the solubility of the ligand and the complexes, despite the presence of four carboxylate groups which stabilize the charge of the complete complex and were intended to improve the solubility of **LnL^2** complexes in water. Consequently, the remaining experiments with **LnL^2** complexes were performed in an acetonitrile/water 1/1 (v/v) solvent mixture.

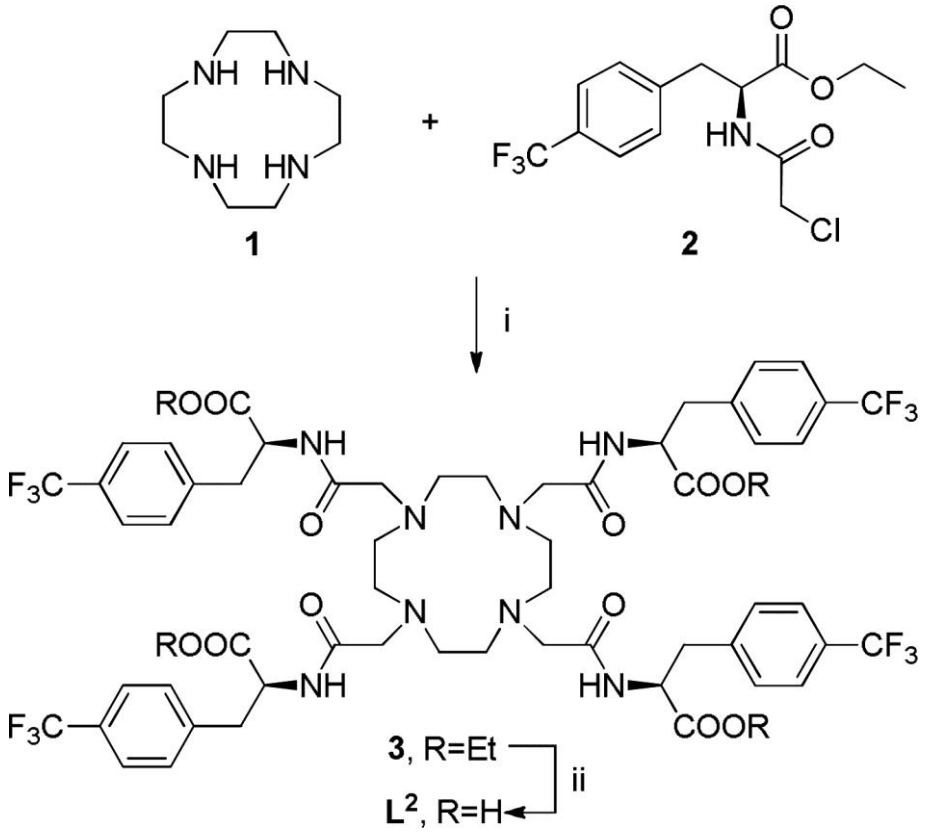

Scheme 1. Preparation of **L**^{2a}

^{a} Reagents and conditions: (i) K_2CO_3, KI, CH_3CN, 70 °C, 18 h, 85%; (ii) NaOH, THF/EtOH/H_2O (3/2/2, v/v/v), 60 °C, 40 h, 93%.

CEST Properties

Our first goal was to investigate the CEST properties of **EuL^1** in detail and perform the qCEST analysis according to the recently reported methodology.[12] Therefore, we performed a series of experiments and recorded Z-spectra at temperatures ranging from 10 to 50 °C, using saturation pulses of different power. In parallel, we have also recorded T_1 and T_2 relaxation times at each temperature. Subsequently, k_{ex} values were calculated using different methods, namely the Bloch–McConnell (BM) differential equations,[17,18] the Omega plot method,[19] and a revised version of quantification of exchange rates as a function of saturation power (QUESP).[12,20]

Qualitative examination of obtained values confirmed the expected trends for T_1 and T_2 relaxation times as a function of sample temperature–while T_1 was elongating with an increase in temperature, the T_2 value was shortened (Figure S1 in the Supporting Information). Similarly, Z-spectra exhibited somewhat expected features, resulting in a sharper and more narrow frequency region with a CEST effect at lower temperatures (consistent with lower k_{ex} values), and broader lines at higher temperatures due to increase in k_{ex} values and stronger magnetization transfer effect.[19] However, temperature-dependent experiments revealed the existence

of two separate peaks at 55 and 58 ppm in the Z-spectrum at 10 °C when using low B_1 fields (10 μT), indicating the presence of two species in solution, both of which demonstrate a CEST effect (Figure 1). These peaks could also be partially recognized at 15 °C at low irradiation powers (10–15 μT), whereas only a single CEST effect could be detected on shifting from 52 to ~40 ppm when changing the temperature from 20 to 50 °C (Figure S2 in the Supporting Information). Similar behavior and separation of CEST peaks was previously observed for other Eu(III) complexes with stereocenters in the δ position, either at lower temperatures (<5 °C) or by using acetonitrile as a solvent.[13-15]

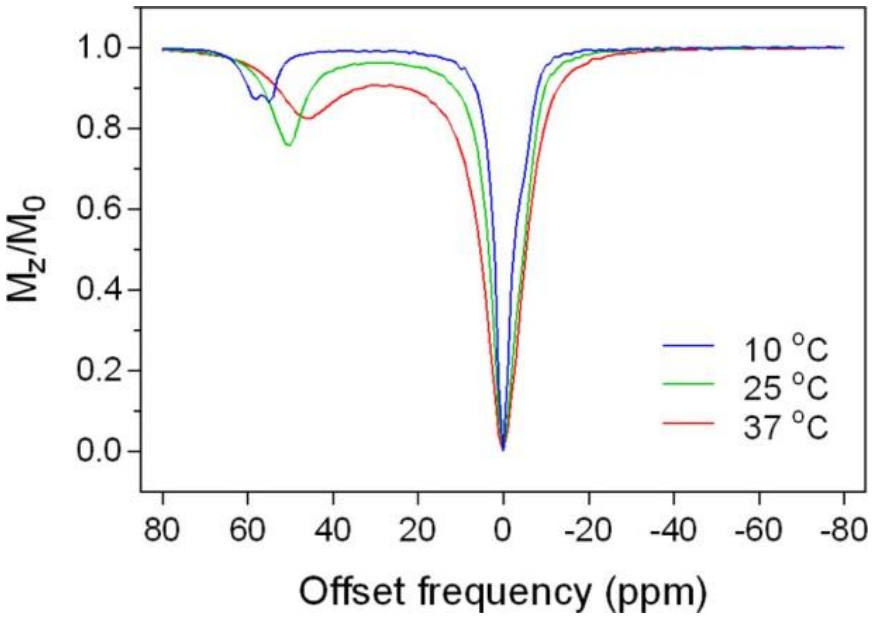

Figure 1. Z-spectra of **EuL^1** (15 mM) at B_1 = 10 μT and irradiation time 10 s at 10, 25, and 37 °C in H_2O/D_2O (9/1, v/v) at pH 7.

qCEST calculations of exchange rates were performed taking into account the high complexity of the **EuL^1** system and were compared to the results that would be obtained assuming a single paraCEST-active species, as the Z-spectrum at room temperature suggests. The revised QUESP or Omega plot methods resulted in k_{ex} values in the ranges of 6.2–6.3 and 10.2–12.8 kHz at 25 and 37 °C, respectively (Table S1 in the Supporting Information). These values differ from our previously reported values for **EuL^1**;[11] the discrepancy originates due to omission of the labeling efficiency term, α, in the initial QUESP formula, or 2π factor in the Omega plot.[12,19,20] Consequently, the previously reported values resulted in lower exchange rates, which still matched well across the quantification methods used.[11] Therefore, we applied a more complex quantification analysis which involved an additional proton exchange pool (Figure 2).[21] However, the fitting of Z-spectra using the BM equations and a four-pool system (exchange of amide protons, bulk water, and the bound water molecules of two isomers) results in different values relative to all other methods (QUESP and Omega plot), including the values obtained from the fitting according to the BM equations assuming three exchanging pools (Figures S2 and S3 in the Supporting Information). Namely, the existence of two species with CEST effects at similar frequencies provides two different k_{ex} values (slower and faster) that can be resolved only with the BM equation assuming four exchanging pools, while the standard and simplified QUESP, Omega plot, or three-pool BM methods assume only one exchanging pool at the given frequency, resulting in a k_{ex} value that is between the actual two values (Table 1; see also Table S1). These observations are unlike those previously reported on other systems with stereogenic centers, in which different k_{ex} values could be separately determined with Omega plots, or with BM equations using two- or three-pool systems.[13,15] Furthermore, calculations performed according to the BM equation provided good

estimates for the fractional concentration of the exchanging species (i.e., paramagnetically shifted water) with values around $\chi \approx 0.00017–0.00018$ that match well with the actual concentrations used in experiments ([**EuL^1**]/[bulk water protons] = 15 mM/2 × 55.5 M). In addition, the obtained fractional concentrations indicated the ratio of isomers ranging from 2/1 to 3/1, depending on the temperature.

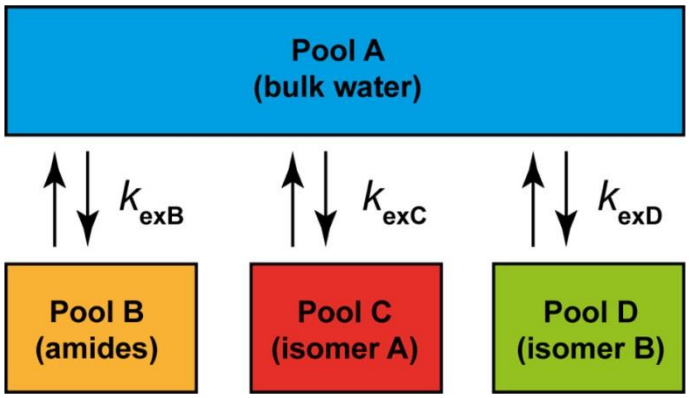

Figure 2. Schematic diagram of the four-pool model which describes the studied exchange processes.

Table 1. Activation Parameters Obtained for **EuL^1** and **EuL^3** According to the Eyring Equation using k_{ex} Values at Different Temperatures and Three Different qCEST Methods[12,17-19]

	qCEST method	k_{ex}^{298} (s^{-1})	$\Delta H^{\ddagger}$ (kJ mol^{-1})	$\Delta S^{\ddagger}$ (J mol^{-1} K^{-1})	$\Delta G^{\ddagger}_{298}$ (kJ mol^{-1})
EuL^1	Bloch 4-pool, isomer A	5228 ± 400	+56.8 ± 1.8	+16.8 ± 5.9	+51.8 ± 2.4
	Bloch 4-pool, isomer B	19009 ± 1900	+57.8 ± 2.3	+31.0 ± 7.7	+48.6 ± 3.1
	Bloch 3-pool	10240 ± 870	+34.7 ± 1.9	–51.9 ± 6.4	+50.2 ± 2.7
	Omega plot	6934 ± 490	+31.9 ± 1.2	–64.3 ± 4.0	+51.1 ± 1.6
	QUESP	6660 ± 600	+22.0 ± 1.4	–97.9 ± 4.6	+51.2 ± 1.9
EuL^3	Bloch 3-pool	7826 ± 120	+55.0 ± 1.1	+14.2 ± 3.7	+50.8 ± 1.9
	Omega plot	6934 ± 67	+54.2 ± 0.7	+10.5 ± 2.2	+51.1 ± 0.9
	QUESP	6396 ± 200	+49.7 ± 1.1	+5.2 ± 3.9	+51.3 ± 1.6

Importantly, the obtained values from four-pool BM equations indicated that species with major abundance are always in a slower exchange regime than the single species of the reference complex **EuL^3** at all temperatures (Figure 3 and Table S1 and Figure S5 in the Supporting Information). This confirms our hypothesis that incorporation of hydrophobic *p*-CF_3-Phe groups results in slower water exchange. On the other hand, the additional chirality generated with these two groups results in a second minor species, which has much faster water exchange, albeit still exhibiting the CEST effect. The k_{ex} values obtained at different temperatures follow an Arrhenius behavior according to eq 1, where R is the gas constant, T is the absolute temperature, E_a is the activation energy, and A is the pre-exponential factor (Figure 3).

$$k_{ex} = Ae^{-E_a/RT} \quad (1)$$

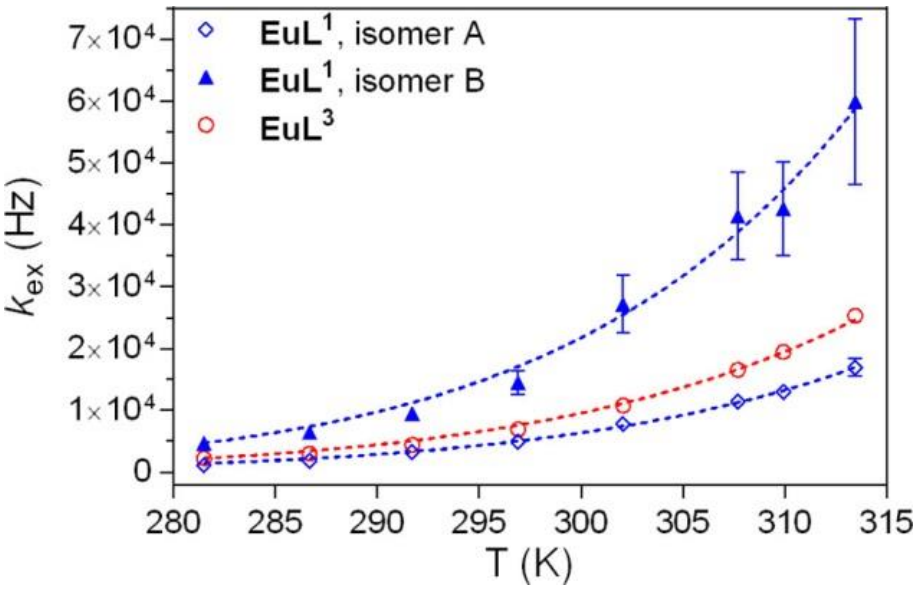

Figure 3. Exchange rate values obtained at different temperatures according to BM equations and four or three exchanging pools for **EuL**^{1} and **EuL**^{3}, respectively. Dashed lines represent fitted values obtained according to the Arrhenius equation.

However, more detailed information on the activation parameters controlling the dynamics of the exchange processes is obtained with the aid of the Eyring equation (eq 2), where k_B and h are the Boltzmann and Planck constants and $\Delta H^{\ddagger}$ and $\Delta S^{\ddagger}$ are the activation enthalpy and activation entropy, respectively.

$$k_{ex} = \frac{k_B T}{h} e^{-\Delta H^{\ddagger}/RT_e - \Delta S^{\ddagger}/R} \qquad (2)$$

The analysis of the CEST spectra of **EuL**^{1} using the BM equation with a four-pool model provided activation parameters characterized by similar activation enthalpies, as anticipated by the nearly parallel trends of the Eyring plots obtained for the two isomers (Figure 4a). Conversely, the rather different intercepts indicated different activation entropies, which nevertheless remain positive (Table 1). However, the three-pool model, Omega plot, and QUESP methods clearly fail to provide reasonable activation parameters, as they give low activation enthalpies and negative activation entropies. Thus, it is clear that a meaningful assessment of the water exchange rates of **EuL**^{1}requires considering the presence of two isomers in solution with rather different water exchange rates of their coordinated water molecules.

In addition to the processes characterized by the three rate constants considered in the four-pool model (Figure 2), the interconversion between the two isomers present in solution (isomers A and B) could be also relevant for the analysis of the data. However, the activation free energies reported in Table 1 fall within a rather narrow range of ~49–52 kJ mol^{-1}. These activation energies are considerably lower than those reported for isomer interconversion of DOTA and DOTA-tetraamide lanthanide complexes, which are typically around 60 kJ mol^{-1}.[22] A barrier of 60 kJ mol^{-1} corresponds to a k_{ex} value of about 200 s^{-1}, which is about 25 times lower than the lowest exchange rate determined in this work. Thus, we conclude that the isomer exchange can be safely neglected for the analysis of the CEST spectra of **EuL**^{1}.

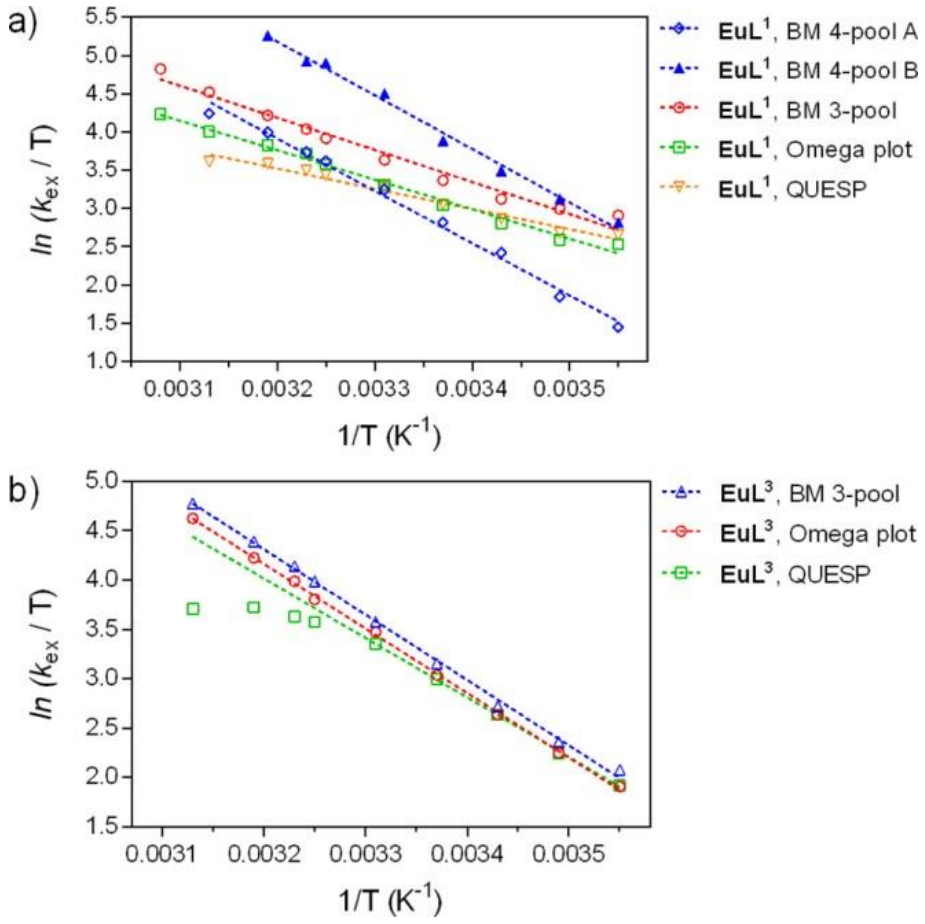

Figure 4. Eyring plots for (a) **EuL^1** (15 mM) and (b) **EuL^3** (10 mM), presenting k_{ex}values obtained at different temperatures with three different qCEST methods.

The activation parameters obtained for **EuL^3** (Table 1) by using the BM and Omega plot methods are in good mutual agreement, while the QUESP methods result in a somewhat lower activation enthalpy, which is compensated by a slightly lower activation entropy. However, the values obtained by the QUESP method must be taken with caution due to the relatively narrow linear range that could be used for the calculation of activation parameters (Figure 4b). This effect is attributed to the limitation of the QUESP method to provide accurate values of fast exchange rates.[23] In contrast, the BM and Omega plot methods provide almost identical activation parameters. Both methods provide positive activation entropies, as expected for water exchange reactions following a dissociatively activated mechanism.[24] The exchange of the coordinated water molecule in lanthanide complexes with octadentate cyclen-based ligands generally follows dissociatively activated mechanisms, which is reflected in positive activation volumes. In the case of **EuL^3**, an activation volume of +4.9 cm^3 mol^{-1} was determined in a CD_3CN/H_2O mixture.[25]

To confirm the observations obtained from **EuL^1**, we have also recorded Z-spectra of **EuL^2** at 25 °C (Figure 5 and Figure S5 in the Supporting Information). In this case, the presence of two species with CEST effects at ~45 and 54 ppm is visible at this temperature, which suggests slower interchange between the species due to higher rigidity (see below). The qCEST performed with three- or four-pool BM fits (excluding or assuming amide protons as an additional exchanging pool) resulted in very similar values, specifically 8177 ± 393 and 3310 ± 406 Hz from a three-pool BM fit for the major and minor species at 45 and 54 pm, respectively, while $\chi \approx 0.000063$ with a 2/1 ratio between the isomers. These values cannot be directly compared to those obtained for **EuL^1** and **EuL^3**, since experiments with **EuL^2** were performed in a different solvent mixture (water/acetonitrile) to enhance solubility. Consequently, k_{ex} values obtained for **EuL^2** are

slower, while the exchange rate of amide protons likely decreases to such an extent that it has no further influence on the exchange processes of paramagnetically shifted protons.

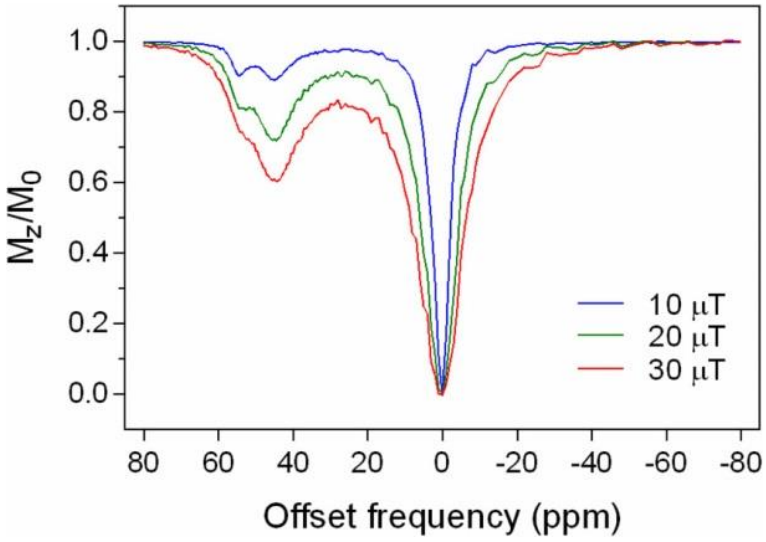

Figure 5. Z-spectra of **EuL^2** (15 mM) at B_1 = 10, 20, and 30 μT and irradiation time 10 s in $H_2O/D_2O/CH_3CN$ (4/1/5, v/v/v) at pH 7 and 25 °C.

Solution Structure

Luminescence Studies.

Luminescence steady-state spectra and lifetime experiments were performed in order to gather additional insights into the coordination properties of the investigated **L^1** system. The steady-state emission spectra of **EuL^1** and **TbL^1** in water (Figure 6) present the characteristic $^5D_0 \rightarrow {}^7F_J$ (J = 0–4) and $^5D_4 \rightarrow {}^7F_J$ (J = 6–3) transitions of Eu(III) and Tb(III), respectively.[26] The emission spectrum of **EuL^1** is very similar to that reported for the analogue with DOTA, which presents a relative population of square-antiprismatic (SAP) and twisted-square-antiprismatic (TSAP) isomers of ∼4/1. Conversely, the TSAP isomers of DOTA and DOTA-tetraamide derivatives present considerably different splitting of the J = 1 and J = 4 manifolds.[27] These results suggest that the population of the **EuL^1** complex in solution is dominated by isomers presenting SAP coordination environments.

The luminescence lifetimes of the $^5D_0$ and $^5D_4$ excited states of **EuL^1** and **TbL^1** were recorded in H_2O and D_2O solutions, and the obtained values were used to estimate hydration numbers for each complex (Table 2). In either of the cases, the results expectedly reveal monohydrated species, with a slightly lower value for **EuL^1** than for **TbL^1** (q = 0.82 and 1.05 for **EuL^1** and **TbL^1**, respectively).

Table 2. Luminescence Lifetimes of **EuL^1** and **TbL^1** in H_2O and D_2O (pH 7, HEPES, 25 °C) and Calculated Hydration Numbers q.

	τ_{H2O} (ms)	τ_{D2O} (ms)	q
EuL^1	0.59	2.18	0.82
TbL^1	1.64	2.95	1.05

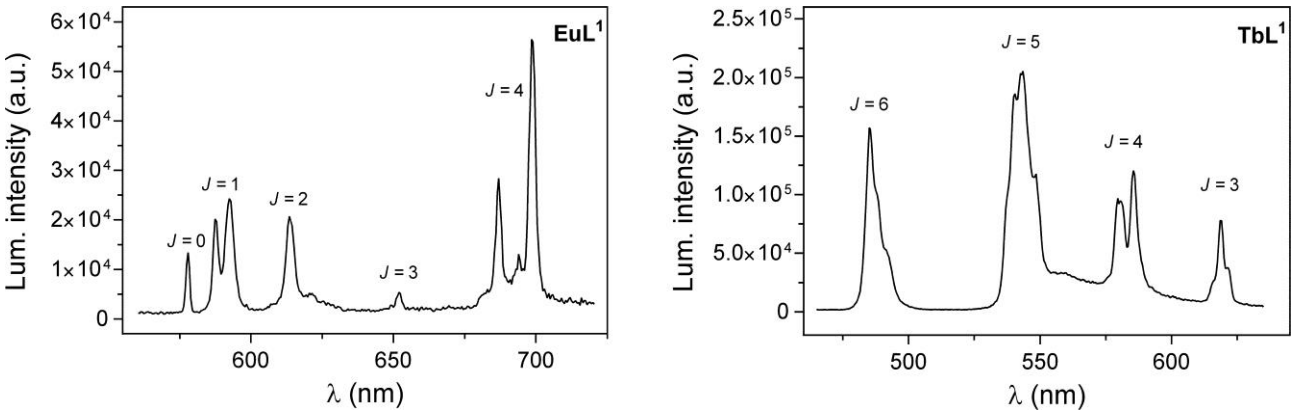

Figure 6. Luminescence emission spectra of **EuL^1** (left, λ_{ex} 395 nm) and **TbL^1** (λ_{ex} 271 nm) at pH 7 (HEPES) and 25 °C.

NMR Studies

The ^{1}H NMR signals of the pseudoaxial protons on the cyclen rings in Eu(III) complexes of DOTA-tetraamide derivatives are usually found above 20–25 ppm in the SAP isomer and below 25 ppm in the TSAP isomer.[28] Consequently, the ^{1}H NMR spectrum of **EuL^1** shows two major signals at 23.8 and 23.6 ppm that we assign to isomer A (Figure S12 in the Supporting Information), the main isomer observed in our CEST experiments (see above). The presence of two signals for the pseudoaxial protons is expected for an effective C_2 symmetry of the complex in solution.[29] The second broad signal that is observed at 25.7 ppm is attributed to isomer B (Figure 7). The highest NMR shift of the axial protons in isomer B is in line with a higher chemical shift of the coordinated water molecule, probably due to a slightly higher pseudocontact contribution in isomer B than in isomer A, as contact contributions of axial protons were found to be generally negligible.[30] Furthermore, isomer A represents about 60% of the overall population of Eu(III) in solution, while the abundance of isomer B represents 25%, which matches well with the BM equation results (see above). The remaining 15% is related to the presence of additional complexes arising from the racemization of the starting amino acid or the pendant arms.[14] The chemical shift range of the pseudoaxial proton in the different species present in solution points to SAP isomers, which is also in line with the chemical shifts observed for the coordinated water molecules of isomers A and B (~50 ppm at room temperature with respect to the bulk water resonance). The ^{1}H NMR spectrum of **EuL^2** is simpler due to the C_4 symmetry of the system and shows two signals at 21.4 and 26.2 ppm that correspond to two SAP diastereoisomers with populations of ca. 72 and 28%, respectively (Figure 7 and Figure S13 in the Supporting Information). Conversely, the spectrum of **EuL^3** is even simpler and presents a single set of signals corresponding to the SAP diastereoisomer (Figure S14 in the Supporting Information).[21]

DFT Calculations

Further insight into the nature of the complex species of **EuL^1** present in aqueous solution was gained with DFT calculations (see Computational Details). These calculations provide two minimum energy structures that correspond to the *SS*-Δ(λλλλ) and *SS*-Λ(δδδδ) isomers, which present capped SAP coordination environments, and two additional minima corresponding to the *SS*-Λ(λλλλ) and *SS*-Δ(δδδδ) isomers, which display capped TSAP geometries (Figure 8 and Tables S2–S5 in the Supporting Information). All four isomers are diastereoisomers as a result of the presence of stereogenic centers in two of the pendant arms, in contrast to the situation observed for complexes such as **LnL^3**, which exist in solution as two diastereoisomeric pairs of enantiomers.[31] The relative energies of the four isomers fall within ~3 kcal mol^{-1}, with the lowest energy conformation corresponding to the SAP *SS*-Δ(λλλλ) form. However, given the accuracy of the energies obtained with our DFT calculations, a precise assignment of the A and B isomers

observed by NMR on the basis of the NMR results is not possible. Nevertheless, we tentatively assign the major isomer present in solution (isomer A) to the *SS*-Λ(δδδδ) diastereoisomer, with the minor isomer (isomer B) being attributed to the *SS*-Δ(λλλλ) isomer. This assignment is made on the basis of (i) the somewhat shorter Eu–O_{water} distance calculated for *SS*-Λ(δδδδ) (2.524 Å) in comparison to *SS*-Δ(λλλλ) (2.537 Å), as shorter Eu–O_{water} distances were found to correlate with lower water exchange rates[32] and (ii) the average Eu···F distance in *SS*-Λ(δδδδ) (10.7 Å) being longer than that calculated for *SS*-Δ(λλλλ) (9.5 Å), which is in line with the broader ^{19}F NMR resonance observed for the latter (20.4 Hz at 25 °C and 7.05 T) in comparison to the former (12.6 Hz under the same conditions, Figure S15 in the Supporting Information).[33] On the basis of these findings, we conclude that both SAP isomers, i.e. *SS*-Λ(δδδδ)/isomer A and *SS*-Δ(λλλλ)/isomer B, are the actual CEST-active species observed in respective experiments (see above), since it is well-known that TSAP isomers present water exchange rates several orders of magnitude higher than those of the corresponding SAP isomers[34] and hence do not display a CEST effect.

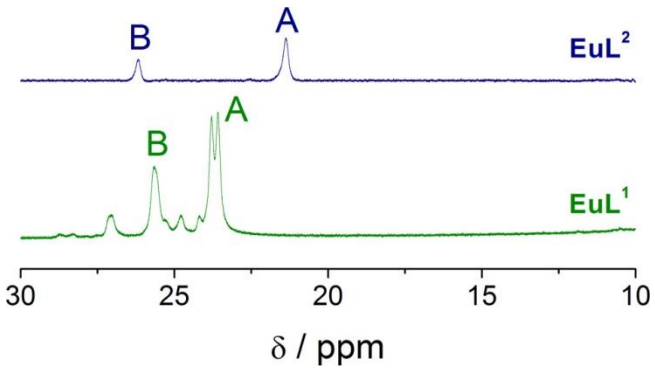

Figure 7. Partial ^{1}H NMR spectra of the **EuL^1** (H_2O/D_2O 9/1, v/v) and **EuL^2** ($H_2O/D_2O/CH_3CN$ 4/1/5, v/v/v) complexes showing the most shifted resonances due to axial protons.

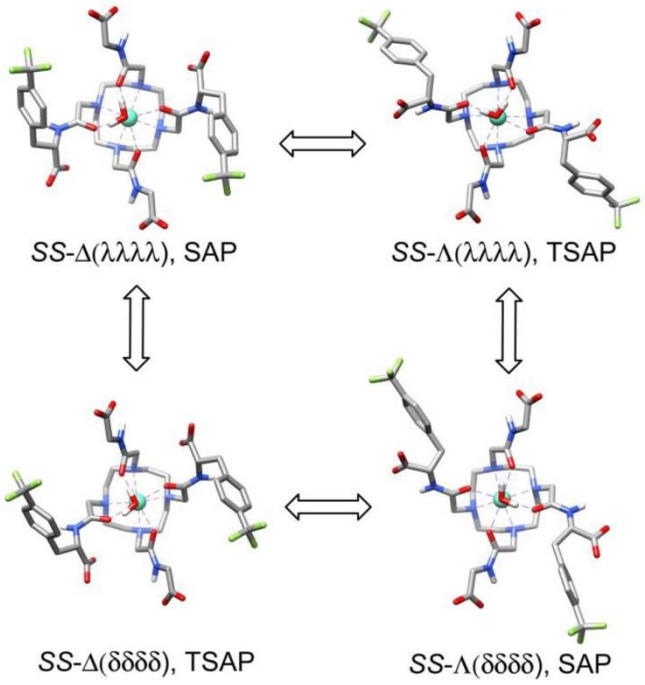

Figure 8. Structures of the four diastereoisomers of **EuL^1** obtained with DFT calculations.

Conclusions

We studied a pair of DOTA-tetraamide complexes **EuL^{1,2}** appended with two or four chiral *p*-CF_3-Phe groups, and compared findings with those for **EuL^3**, the DOTAM-type complex with four achiral glycineamide groups. A detailed investigation using luminescence, NMR, and DFT studies shows that the isomeric composition of the **EuL^1** complex in solution is dominated by the *SS*-Δ(λλλλ) and *SS*-Λ(δδδδ) stereoisomers, which present capped SAP coordination environments. As a result of the similar coordination environments, and thus magnetic anisotropies, the ^{1}H NMR signals of the coordinated water molecules of the two isomers present very similar chemical shifts. Thus, two separate signals are only observed in Z-spectra at low temperatures when low irradiation powers are used, similar to previously conducted studies with other side arms containing stereocenters in the δ position.[13-15] However, in this work we extract different k_{ex}values directly from aqueous solutions at a wide range of temperatures without the need to separate CEST peaks by using other solvents or lower temperatures.[13-15] The assessment of the water exchange rates of the two coordinated water molecules shows that one of the isomers present in solution (presumably the *SS*-Δ(λλλλ) form) has a water exchange rate 4–5 times higher than that of the second isomer. The results reported in this paper clearly demonstrate that the water exchange rates of two SAP isomers with the same ligand might also differ significantly, a property that must be considered when performing quantification of CEST results. Consequently, the use of methods that neglect the presence of two paramagnetic water exchanging species, such as the single-pool QUESP and Omega plot methods, can result in erroneous water exchange rates and activation parameters.

Experimental Section

General Remarks

Commercially available reagents and solvents were used with no further purification. Compounds **2**, **EuL^1**, **TbL^1**, and **EuL^3** were prepared according to previously reported procedures.[11, 16] Purification of the synthesized compounds was performed using silica gel 60 (0.03–0.2 mm) from Carl Roth (Germany). All NMR data were acquired on a Bruker Avance III 300 MHz spectrometer using deuterium lock frequency, processed with TopSpin 2.1 (Bruker GmbH), and analyzed with TopSpin 2.1 or ACD/SpecManager 9.0 (Advanced Chemistry Development, Inc.). The spectra of lanthanide complexes were recorded using samples in H_2O/D_2O (9/1, v/v) for **LnL^1** (15 mM) and **LnL^3** (10 mM) or $H_2O/D_2O/CH_3CN$ (4/1/5, v/v/v) for **LnL^2** (15 mM). The bulk magnetic susceptibility shift (BMS) was used to determine the concentration of complexes.[35] ESI-HRMS was performed on a Bruker BioApex II ESI-FT-ICR, equipped with an Agilent ESI source, measured via flow injection analysis. ESI-LRMS was performed on an ion trap SL1100 system (Agilent, Germany).

Synthesis of L^2

Compound 3. Cyclen (**1**; 66 mg, 0.38 mmol), K_2CO_3 (237 mg, 1.71 mmol), and KI (45 mg, 0.27 mmol) were mixed in acetonitrile (30 mL) and stirred for 30 min. A solution of **2** (644 mg, 1.91 mmol) in acetonitrile (10 mL) was added to the reaction mixture in 2 mL portions every 45 min. The reaction mixture was heated to 70 °C after the first addition and stirred at 70 °C for 18 h after the last addition, after which time the mixture was cooled, filtered, and concentrated. The crude product was purified using column chromatography (silica gel, 20% EtOAc in CH_2Cl_2 followed by 1–5% MeOH in DCM) to yield macrocycle **3** (460 mg, 88%) as a yellow oil. ^{1}H NMR ($CDCl_3$, 300 MHz): δ (ppm) 7.54 (d, *J* = 7.1 Hz, 8 H), 7.38 (d, *J* = 7.9 Hz, 8 H), 7.06–6.77 (br, 4 H), 4.95–4.74 (br, 4 H), 4.26–4.04 (br, 8 H), 3.33–1.56 (br, 32 H), 1.34–1.11 (br, 12 H). ^{13}C{^{1}H} NMR ($CDCl_3$, 75 MHz): δ (ppm) 172.1, 170.8, 170.5, 141.0, 129.9, 129.5, 128.5 (q, *J* = 32.2 Hz), 124.8 (q, *J* = 3.2 Hz), 123.9 (q, *J* = 272.9 Hz), 61.2, 57.5, 55.9, 52.5, 52.3, 50.4, 37.5, 17.9, 13.7, 13.6. ^{19}F{^{1}H}

NMR ($CDCl_3$, 282 MHz): δ (ppm) −62.1 (br), −62.4. HR-ESI$^+$/MS (*m*/*z*): for $C_{64}H_{77}F_{12}N_8O_{12}^+$, calcd 1377.5464 $[M + H]^+$, found 1377.5440.

***L*^{2}**. The macrocycle **3** (319 mg, 0.23 mmol) was dissolved in a mixture of EtOH (1 mL) and THF (1.5 mL). A solution of NaOH (74 mg, 1.86 mmol) in H_2O (1 mL) was added dropwise, and the mixture was stirred at 60 °C for 40 h. THF and EtOH were removed by rotary evaporation; the mixture was acidified to pH 2 using 1 M HCl, and then the solvent was removed. The product was purified by addition of EtOH (10 mL) and removal of solid (NaCl) by filtration and evaporation. The product was then washed with water (3 × 10 mL) to give the tetraacid **L^2** (272 mg, 93%) as a pale yellow solid. ^{1}H NMR (CD_3OD, 300 MHz): δ (ppm) 7.72–7.49 (m, 8 H), 7.48–7.32 (m, 8 H), 4.80–4.63 (br, 4 H), 3.68–2.48 (br, 32 H). ^{13}C{^{1}H} NMR (CD_3OD, 75 MHz): δ (ppm) 174.8, 174.6, 143.5, 131.5, 131.2, 130.0 (q, *J* = 32.6 Hz), 126.3 (q, J = 3.3 Hz), 125.8 (q, *J* = 271.2 Hz), 62.8, 62.5, 57.0 (br), 55.4, 52.6 (br), 50.0, 38.3. ^{19}F{^{1}H} NMR (CD_3OD, 282 MHz): δ (ppm) −63.1, −63.5. HR-ESI$^-$/MS (*m*/*z*): for $C_{56}H_{59}F_{12}N_8O_{12}^-$, calcd 1263.4066 $[M - H]^-$, found 1263.4074.

General Procedure for Preparation of Ln^{3+} Complexes

The ligand **L^2** (0.020 mmol) was suspended in EtOH (5 mL). A solution of $LnCl_3 \cdot 6H_2O$ (0.024 mmol) in H_2O (5 mL) was added, while the pH was adjusted to 7.0–7.5 using 0.1 M NaOH, and the mixture was stirred at 60 °C for 24 h. After this time Chelex 100 was added and the mixture was stirred at 60 °C for a further 12 h. The reaction mixture was cooled and filtered, and EtOH was removed by rotary evaporation. The pH was adjusted to 7.0–7.5 using 0.1 M HCl and H_2O evaporated to yield the desired complex. HR-ESI$^-$/MS (*m*/*z*): for $C_{56}H_{56}EuF_{12}N_8O_{12}^-$ (**EuL^2**), calcd 1413.3044 $[M - H]^-$, found 1413.3068; for $C_{56}H_{56}F_{12}N_8O_{12}Yb^-$ (**YbL^2**), calcd 1434.3220 $[M-H]^-$, found 1434.3250; for $C_{56}H_{56}DyF_{12}N_8O_{12}^-$ (**DyL^2**), calcd 1424.3123 $[M-H]^-$, found 1424.3144.

CEST Experiments

The saturation transfer experiments were carried out in the temperature range 10–50 °C by irradiating the sample at increments of 1 ppm in the frequency range ±80 or ±100 ppm. Spectra were measured by recording the bulk water signal intensity as a function of the presaturation frequency. Saturation offsets are reported relative to the signal of bulk water. The used temperatures were corrected by measuring the frequency difference of neat ethylene glycol at each temperature reported.[36]

For each temperature, data were collected by varying the saturation power while the saturation time remained constant (10 s). The saturation field strengths varied between 425 and 1490 Hz: specifically 10, 15, 20, 25, 30, and 35 μT. The data were fitted using the self-written script in MatLab (version R2016b, MathWorks, USA) according to recently reported procedures.[12] Longitudinal and transverse relaxation times were obtained in independent experiments (inversion recovery and Carr–Purcell–Meiboom–Gill experiments for T_1 and T_2, respectively).

Multi-B_1-Z-spectra were fitted simultaneously using the numerical solution of the Bloch–McConnell equations,[18] assuming a four-pool system with starting parameters and boundaries for the least-squares optimization as given in Table 3. Each pool *i* is defined by the relaxation rates R_{1i} and R_{2i}. The fractional concentration, χ_i, represents the ratio of concentration of exchanging protons in the particular pool (which is equal to inner-sphere water or concentration of lanthanide complex) and total proton concentration in bulk water (2 × 55.5 M), i.e. $\chi = (15 \times 10^{-3}\ M)/(111\ M) = 0.000135$, while the $k_{ex,i}$ and $\delta\omega_i$ values are the exchange rates and the chemical shifts of these pools, respectively.

Table 3. Parameters of the Four-Pool System BM Fit of **EuL^1** [a]

param	start value	lower bound	upper bound
$\delta\omega_A$	0	–1	1
$R_{2,A}$	0.5000	0.166667	10000
$\delta\omega_B$	–6	–10	10
χ_B	0.0005	0.000486	0.000595
$k_{ex,B}$	50	10	10000
$R_{2,B}$	50	1	50
$\delta\omega_C$	55	50	65
χ_C	0.0001	0.0000135	0.00135
$k_{ex,C}$	2000	50	1500000
$R_{2,C}$	50	0.050000	50
$\delta\omega_D$	54	39	69
χ_D	0.0001	0	0.01
$k_{ex,D}$	10000	10	2500000
$R_{2,D}$	50	0.050000	50

[a] Pool A, bulk water; pool B, amides; pools C and D, **EuL^1** isomers. Fixed values used:$R_{1,A}$ was measured by inversion recovery and provided to the fit. $R_{1,B} = R_{1,C} = R_{1,D} = 0$.

^{1}H NMR Experiments with LnL$^{1–3}$ Complexes

The spectra were recorded on 15 mM samples in H_2O/D_2O (9/1, v/v) for **LnL^1** and **LnL^3** or $H_2O/D_2O/CH_3CN$ (4/1/5, v/v/v) for **LnL^2** using the deuterium frequency to lock the signal. A series of ^{1}H NMR experiments were performed using one or more of the following pulse programs: (1) the standard pulse sequence with the 30° pulse, (2) the sequence with weak presaturation pulse at water frequency to cause the suppression of water or acetonitrile signals, and (3) the sequence with water suppression by gradient tailored excitation (WATERGATE) in order to reduce the signal of water in an attempt to detect the bound water.

Luminescence Experiments

The lifetime measurements were performed on a QuantaMasterTM 3 PH fluorescence spectrometer from Photon Technology International, Inc. The measurements were performed in H_2O and D_2O (25 °C) at the same **EuL^1** or **TbL^1** concentrations (5 mM). The Eu(III) ion was directly excited at 395 nm, and the emission intensity at 595 nm was measured with a 10 μs resolution. The excitation and emission slits were set to 28 and 10 nm band pass, respectively. The Tb(III) ion was directly excited at 271 nm, and the emission intensity at 546 nm was measured with a 10 μs resolution. The excitation and emission slits were set to 15 and 5 nm band pass, respectively. Data sets are an average of 25 scans, and each reported value is the mean of three independent measurements. The obtained curves were fitted to a first-order exponential decay with $r^2 = 0.99$. The q values were calculated using eqs 3 and 4 for **EuL^1** and **TbL^1**, respectively.[37]

$$q_{\mathrm{Eu}} = 1.2 \times [(k_{\mathrm{H2O}} - k_{\mathrm{D2O}}) - 0.25 + 0.075 n_{\mathrm{O=CNH}}] \quad n = 4 \qquad (3)$$

$$q_{\mathrm{Tb}} = 5 \times [(k_{\mathrm{H2O}} - k_{\mathrm{D2O}}) - 0.06] \qquad (4)$$

Computational Details

Full geometry optimizations of the **EuL^1** system were performed in aqueous solution employing DFT within the hybrid meta-GGA approximation with the TPSSh exchange-correlation functional[38] and the Gaussian 09 package (Revision D.01).[39] In these calculations we used the large-core relativistic effective core potential (LCRECP) of Dolg et al. and the related [5s4p3d]-GTO valence basis set for Eu,[40] together with the standard 6-31G(d) basis set for C, H, F, N, and O atoms. Since the LCRECP approach includes 46 + 4f^6 electrons of Eu(III) in the core, calculations were conducted on a pseudo singlet state configuration. No symmetry constraints were imposed during the optimizations. The default values for the integration grid (75 radial shells and 302 angular points) and the SCF energy convergence criteria (10^{-8}) were used in all calculations. The stationary points found on the potential energy surfaces were tested to represent energy minima rather than saddle points via frequency analysis (0 imaginary frequencies). Solvent effects (water) were included by using the integral equation formalism variant of the polarizable continuum model (IEFPCM),[41] as implemented in Gaussian 09.

Associated Content

Supporting Information

The Supporting Information is available free of charge on the ACS Publications website at DOI: 10.1021/acs.inorgchem.7b00441.

- CEST spectra and water exchange rate constants determined at different temperatures, ^{1}H and ^{19}F NMR spectra, and optimized (DFT) Cartesian coordinates (PDF).

Notes

The authors declare no competing financial interest.

Acknowledgments

The authors acknowledge financial support of the Max Planck Society, Ministerio de Economía y Competitivad (CTQ2015-71211-REDT and CTQ2013-43243-P, support to C.P.-I. and D.E.-G.), Santander International Connections Award (support to B.T.), German Research Foundation (DFG, grant ZA 814/2-1, support to M.Z.), European Union's Horizon 2020 research and innovation programme (Grant Agreement No. 667510, support to M.Z.), and Centro de Supercomputación de Galicia (CESGA) for providing the computer facilities.

References

(1) Tóth, É.; Helm, L.; Merbach, A. In *The Chemistry of Contrast Agents in Medical Magnetic Resonance Imaging*; Wiley: Chichester, U.K., 2013; pp 25−81.

(2) Yu, J.-X.; Hallac, R. R.; Chiguru, S.; Mason, R. P. New frontiers and developing applications in ^{19}F NMR. *Prog. Nucl. Magn. Reson. Spectrosc*. **2013**, *70*, 25−49.

(3) Matsushita, H.; Mizukami, S.; Sugihara, F.; Nakanishi, Y.; Yoshioka, Y.; Kikuchi, K. Multifunctional Core-Shell Silica Nanoparticles for Highly Sensitive ^{19}F Magnetic Resonance Imaging. *Angew. Chem., Int. Ed*. **2014**, *53* (4), 1008−1011.

(4) van Zijl, P. C. M.; Yadav, N. N. Chemical Exchange Saturation Transfer (CEST): What is in a Name and What Isn't? *Magn. Reson. Med*. **2011**, *65* (4), 927−948.

(5) Sherry, A. D.; Wu, Y. K. The importance of water exchange rates in the design of responsive agents for MRI. *Curr. Opin. Chem. Biol*. **2013**, *17* (2), 167−174.

(6) Terreno, E.; Castelli, D. D.; Aime, S. In *The Chemistry of Contrast Agents in Medical Magnetic Resonance Imaging*; Wiley: Chichester, U.K., 2013; pp 387−425.

(7) Cockerill, A. F.; Davies, G. L. O.; Harden, R. C.; Rackham, D. M. Lanthanide Shift Reagents for Nuclear Magnetic-Resonance Spectroscopy. *Chem. Rev*. **1973**, *73* (6), 553−588.

(8) Geraldes, C. F. G. C.; Luchinat, C. In *Metal Ions in Biological Systems: The lanthanides and their interrelations with biosystems*; Sigel, H., Sigel, A., Eds.; Marcel Dekker: New York, 2003; Chapter 14, Vol. 40, pp 513−588.

(9) Olatunde, A. O.; Dorazio, S. J.; Spernyak, J. A.; Morrow, J. R. The NiCEST Approach: Nickel(II) ParaCEST MRI Contrast Agents. *J. Am. Chem. Soc*. **2012**, *134* (45), 18503−18505.

(10) Fernando, W. S.; Martins, A. F.; Zhao, P.; Wu, Y.; Kiefer, G. E.; Platas-Iglesias, C.; Sherry, A. D. Breaking the Barrier to Slow Water Exchange Rates for Optimal Magnetic Resonance Detection of paraCEST Agents. *Inorg. Chem*. **2016**, *55* (6), 3007−3014.

(11) Cakic, N.; Savic, T.; Stricker-Shaver, J.; Truffault, V.; Platas-´ Iglesias, C.; Mirkes, C.; Pohmann, R.; Scheffler, K.; Angelovski, G. Paramagnetic lanthanide chelates for multicontrast MRI. *Chem. Commun*. **2016**, *52* (59), 9224−9227.

(12) Zaiss, M.; Angelovski, G.; Demetriou, E.; McMahon, M. T.; Golay, X.; Scheffler, K. QUESP and QUEST revisited − fast and accurate quantitative CEST experiments. *Magn. Reson. Med*. **2017**, DOI: 10.1002/mrm.26813.

(13) Carney, C. E.; Tran, A. D.; Wang, J.; Schabel, M. C.; Sherry, A. D.; Woods, M. Towards the Rational Design of MRI Contrast Agents: delta-Substitution of Lanthanide(III) NB-DOTA-Tetraamide Chelates Influences but Does Not Control Coordination Geometry. *Chem. - Eur. J*. **2011**, *17* (37), 10372−10378.

(14) Mani, T.; Opina, A. C. L.; Zhao, P. Y.; Evbuomwan, O. M.; Milburn, N.; Tircso, G.; Kumas, C.; Sherry, A. D. The stereochemistry of amide side chains containing carboxyl groups influences water exchange rates in EuDOTA-tetraamide complexes. *JBIC, J. Biol. Inorg. Chem*. **2014**, *19* (2), 161−171.

(15) Slack, J. R.; Woods, M. The effect of regioisomerism on the coordination chemistry and CEST properties of lanthanide(III) NBDOTA-tetraamide chelates. *JBIC, J. Biol. Inorg. Chem*. **2014**, *19* (2), 173−189.

(16) Aime, S.; Barge, A.; Delli Castelli, D.; Fedeli, F.; Mortillaro, A.; Nielsen, F. U.; Terreno, E. Paramagnetic lanthanide(III) complexes as pH-sensitive chemical exchange saturation transfer (CEST) contrast agents for MRI applications. *Magn. Reson. Med*. **2002**, *47* (4), 639− 648.

(17) McConnell, H. M. Reaction Rates by Nuclear Magnetic Resonance. *J. Chem. Phys*. **1958**, *28* (3), 430−431.

(18) Woessner, D. E.; Zhang, S. R.; Merritt, M. E.; Sherry, A. D. Numerical solution of the Bloch equations provides insights into the optimum design of PARACEST agents for MRI. *Magn. Reson. Med*. **2005**, *53* (4), 790−799.

(19) Dixon, W. T.; Ren, J. M.; Lubag, A. J. M.; Ratnakar, J.; Vinogradov, E.; Hancu, I.; Lenkinski, R. E.; Sherry, A. D. A Concentration-Independent Method to Measure Exchange Rates in PARACEST Agents. *Magn. Reson. Med*. **2010**, *63* (3), 625−632.

(20) McMahon, M. T.; Gilad, A. A.; Zhou, J. Y.; Sun, P. Z.; Bulte, J. W. M.; van Zijl, P. C. M. Quantifying exchange rates in chemical exchange saturation transfer agents using the saturation time and saturation power dependencies of the magnetization transfer effect on the magnetic resonance imaging signal (QUEST and QUESP): pH calibration for poly-L-lysine and a starburst dendrimer. *Magn. Reson. Med.* **2006**, *55* (4), 836−847.

(21) Li, A. X.; Hudson, R. H. E.; Barrett, J. W.; Jones, C. K.; Pasternak, S. H.; Bartha, R. Four-Pool Modeling of Proton Exchange Processes in Biological Systems in the Presence of MRI-Paramagnetic Chemical Exchange Saturation Transfer (PARACEST) Agents. *Magn. Reson. Med*. **2008**, *60* (5), 1197−1206.

(22) Platas-Iglesias, C. The Solution Structure and Dynamics of MRI Probes Based on Lanthanide(III) DOTA as Investigated by DFT and NMR Spectroscopy. *Eur. J. Inorg. Chem.* **2012**, *2012*, 2023−2033.

(23) Randtke, E. A.; Chen, L. Q.; Corrales, L. R.; Pagel, M. D. The Hanes-Woolf Linear QUESP Method Improves the Measurements of Fast Chemical Exchange Rates with CEST MRI. *Magn. Reson. Med*. **2014**, *71* (4), 1603−1612.

(24) Helm, L.; Merbach, A. E. Inorganic and bioinorganic solvent exchange mechanisms. *Chem. Rev*. **2005**, *105* (6), 1923−1959.

(25) Dunand, F. A.; Dickins, R. S.; Parker, D.; Merbach, A. E. Towards Rational Design of Fast Water-Exchanging Gd(dota-like) Contrast Agents? Importance of the M/m Ratio. *Chem. - Eur. J*. **2001**, *7* (23), 5160−5167.

(26) Eliseeva, S. V.; Bunzli, J. C. G. Lanthanide luminescence for functional materials and bio-sciences. *Chem. Soc. Rev*. **2010**, *39* (1), 189−227.

(27) Woods, M.; Aime, S.; Botta, M.; Howard, J. A. K.; Moloney, J. M.; Navet, M.; Parker, D.; Port, M.; Rousseaux, O. Correlation of water exchange rate with isomeric composition in diastereoisomeric gadolinium complexes of tetra(carboxyethyl)dota and related macrocyclic ligands. *J. Am. Chem. Soc*. **2000**, *122* (40), 9781−9792.

(28) Kumas, C.; Fernando, W. S.; Zhao, P. Y.; Regueiro-Figueroa, M.; Kiefer, G. E.; Martins, A. F.; Platas-Iglesias, C.; Sherry, A. D. Unexpected Changes in the Population of Coordination Isomers for the Lanthanide Ion Complexes of DOTMA-Tetraglycinate. *Inorg. Chem*. **2016**, *55* (18), 9297−9305.

(29) Lima, L. M. P.; Lecointre, A.; Morfin, J. F.; de Blas, A.; Visvikis, D.; Charbonniere, L. J.; Platas-Iglesias, C.; Tripier, R. Positively Charged Lanthanide Complexes with Cyclen-Based Ligands: Synthesis, Solid-State and Solution Structure, and Fluoride Interaction. *Inorg. Chem*. **2011**, *50* (24), 12508−12521.

(30) Rodriguez-Rodriguez, A.; Esteban-Gomez, D.; de Blas, A.; Rodriguez-Blas, T.; Botta, M.; Tripier, R.; Platas-Iglesias, C. Solution Structure of Ln(III) Complexes with Macrocyclic Ligands Through Theoretical Evaluation of H-1 NMR Contact Shifts. *Inorg. Chem*. **2012**, *51* (24), 13419−13429.

(31) Parker, D.; Dickins, R. S.; Puschmann, H.; Crossland, C.; Howard, J. A. K. Being excited by lanthanide coordination complexes: Aqua species, chirality, excited-state chemistry, and exchange dynamics. *Chem. Rev*. **2002**, *102* (6), 1977−2010.

(32) Regueiro-Figueroa, M.; Platas-Iglesias, C. Toward the Prediction of Water Exchange Rates in Magnetic Resonance Imaging Contrast Agents: A Density Functional Theory Study. *J. Phys. Chem. A* **2015**, *119* (24), 6436−6445.

(33) Aime, S.; Barbero, L.; Botta, M.; Ermondi, G. Determination of Metal Proton Distances and Electronic Relaxation-Times in Lanthanide Complexes by Nuclear-Magnetic-Resonance Spectroscopy. *J. Chem. Soc., Dalton Trans.* **1992**, *2*, 225−228.

(34) Dunand, F. A.; Aime, S.; Merbach, A. E. First ^{17}O NMR Observation of Coordinated Water on Both Isomers of [Eu-(DOTAM)$(H_2O)]^{3+}$: A direct access to water exchange and its role in the isomerization. *J. Am. Chem. Soc*. **2000**, *122* (7), 1506−1512.

(35) Corsi, D. M.; Platas-Iglesias, C.; van Bekkum, H.; Peters, J. A. Determination of paramagnetic lanthanide(III) concentrations from bulk magnetic susceptibility shifts in NMR spectra. *Magn. Reson. Chem*. **2001**, *39* (11), 723−726.

(36) Ammann, C.; Meier, P.; Merbach, A. E. A Simple Multi-Nuclear NMR Thermometer. *J. Magn. Reson*. **1982**, *46* (2), 319−321.

(37) Beeby, A.; Clarkson, I. M.; Dickins, R. S.; Faulkner, S.; Parker, D.; Royle, L.; de Sousa, A. S.; Williams, J. A. G.; Woods, M. Nonradiative deactivation of the excited states of europium, terbium and ytterbium complexes by proximate energy-matched OH, NH and CH oscillators: an improved luminescence method for establishing solution hydration states. *J. Chem. Soc., Perkin Trans. 2* **1999**, No. 3, 493−503.

(38) Tao, J. M.; Perdew, J. P.; Staroverov, V. N.; Scuseria, G. E. Climbing the density functional ladder: Nonempirical meta-generalized gradient approximation designed for molecules and solids. *Phys. Rev. Lett*. **2003**, *91* (14), 146401.

(39) Frisch, M. J.; Trucks, G. W.; Schlegel, H. B.; Scuseria, G. E.; Robb, M. A.; Cheeseman, J. R.; Scalmani, G.; Barone, V.; Mennucci, B.; Petersson, G. A.; Nakatsuji, H.; Caricato, M.; Li, X.; Hratchian, H. P.; Izmaylov, A. F.; Bloino, J.; Zheng, G.; Sonnenberg, J. L.; Hada, M.; Ehara, M.; Toyota, K.; Fukuda, R.; Hasegawa, J.; Ishida, M.; Nakajima, T.; Honda, Y.; Kitao, O.; Nakai, H.; Vreven, T.; Montgomery, J. A.; Peralta, J. E.; Ogliaro, F.; Bearpark, M.; Heyd, J. J.; Brothers, E.; Kudin, K. N.; Staroverov, V. N.; Kobayashi, R.; Normand, J.; Raghavachari, K.; Rendell, A.; Burant, J. C.; Iyengar, S. S.; Tomasi, J.; Cossi, M.; Rega, N.; Millam, J. M.; Klene, M.; Knox, J. E.; Cross, J. B.; Bakken, V.; Adamo, C.; Jaramillo, J.; Gomperts, R.; Stratmann, R. E.; Yazyev, O.; Austin, A. J.; Cammi, R.; Pomelli, C.; Ochterski, J. W.; Martin, R. L.; Morokuma, K.; Zakrzewski, V. G.; Voth, G. A.; Salvador, P.; Dannenberg, J. J.; Dapprich, S.; Daniels, A. D.; Farkas; Foresman, J. B.; Ortiz, J. V.; Cioslowski, J.; Fox, D. J. *Gaussian 09, Revision B.01*, Gaussian, Inc., Wallingford, CT, 2009.

(40) Dolg, M.; Stoll, H.; Savin, A.; Preuss, H. Energy-Adjusted Pseudopotentials for the Rare-Earth Elements. *Theor. Chim. Acta* **1989**, *75* (3), 173−194.

(41) Tomasi, J.; Mennucci, B.; Cammi, R. Quantum mechanical continuum solvation models. *Chem. Rev.* **2005**, *105* (8), 2999−3093.